Journal of Hazardous Materials 482 (2025) 136609

Contents lists available at ScienceDirect

Journal of Hazardous Materials

journal homepage: www.elsevier.com/locate/jhazmat

# Comprehensive elemental and physical characterization of vehicle brake wear emissions from two different brake pads following the Global Technical Regulation methodology

Carsten Neukirchen [a,b], Mohammad Reza Saraji-Bozorgzad [a], Michael Mäder [c], Ajit Paul Mudan [a], Philipp Czasch [c], Johannes Becker [b,d], Sebastiano Di Bucchianico [b,d,e], Christian Trapp [f], Ralf Zimmermann [b,d,e], Thomas Adam [a,d,*]

[a] University of the Bundeswehr Munich, Faculty for Mechanical Engineering, Institute of Chemistry and Environmental Engineering, Werner-Heisenberg-Weg 39, 85577 Neubiberg, Germany
[b] Joint Mass Spectrometry Center at Chair of Analytical Chemistry, Institute of Chemistry, University of Rostock, Albert-Einstein-Strasse 27, 18059 Rostock, Germany
[c] HDC Blueprints GmbH, Am Hohen Rain 4, 86529 Schrobenhausen, Germany
[d] Joint Mass Spectrometry Center at Comprehensive Molecular Analytics (CMA), Environmental Health Center, Helmholtz Munich, Ingolstädter Landstrasse 1, 85764 Neuherberg, Germany
[e] Department Life, Light & Matter, University of Rostock, Albert Einstein Strasse 25, 18059 Rostock, Germany
[f] University of the Bundeswehr Munich, Faculty for Mechanical Engineering, Institute of Energy and Power Train Technology, Werner-Heisenberg-Weg 39, 85577 Neubiberg, Germany

## HIGHLIGHTS

- $PM_{10}$ emission factors defined for two brake pads.
- More than half of the mass of $PM_{10}$ emitted as iron.
- Geometric mean diameter found in the nanometer range.
- High emissions of heavy metals such as Fe, Cu, Cr, Sn, Mn and Zn.
- Large emission contribution from wear of the brake disc observed.

## GRAPHICAL ABSTRACT

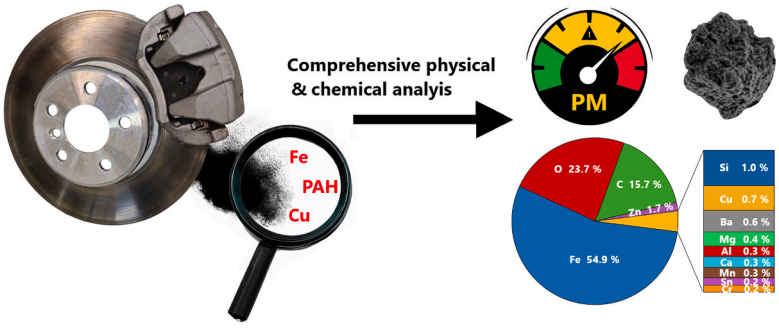


*Abbreviations:* ALI, Air-liquid interface; CPC, Condensation particle counter; CVS, Constant volume sampler; EDX, Energy-dispersive X-ray spectroscopy; GMD, Geometric mean diameter; GTR24, United Nations global technical regulation No.24; ICP-MS/MS, Inductively coupled plasma tandem mass spectrometry; ILS II, Global interlaboratory study; LM, Low metallic; NAO, Non-asbestos organic; NEE, Non-exhaust emissions; OEM, Original equipment manufacturer; OPS, Optical particle sizer; PAH, Polycyclic aromatic hydrocarbons; PC, Polycarbonate; PM, Particulate matter; PMP, Particle measurement programme; PNC, Particle number concentration; ROS, Reactive oxygen species; SEM, Scanning electron microscopy; SI, Supplementary information; SPC, Solid particle counter; SPN, Solid particle number; TPC, Total particle counter; TPN, Total particle number; UNECE, United Nations Economic Commission for Europe; WLTP, Worldwide Harmonized Light Vehicle Test Procedure; BR1Fa, ILS II brake 1 with brake pad a; BR1Fb, ILS II brake 1 with brake pad b.

* Corresponding author at: University of the Bundeswehr Munich, Faculty for Mechanical Engineering, Institute of Chemistry and Environmental Engineering, Werner-Heisenberg-Weg 39, 85577 Neubiberg, Germany,.
*E-mail address:* thomas.adam@unibw.de (T. Adam).

https://doi.org/10.1016/j.jhazmat.2024.136609
Received 26 September 2024; Received in revised form 14 November 2024; Accepted 19 November 2024
Available online 20 November 2024

ARTICLE INFO

*Keywords:*
EURO 7
GTR24
Brake wear
Non-exhaust emissions
Inductively coupled plasma mass spectrometry
Scanning electron microscopy
Chemical composition

ABSTRACT

Non-exhaust emissions have gained increasing attention during the last years, with the upcoming EURO 7 regulation defining maximum $PM_{10}$ emission factors for tire and brake emissions for the first time. This study, therefore, focusses on broadening the knowledge on chemical composition and physical characteristics of brake dust to define emission factors for heavy metal and organic pollutants. Particles from two pads were analyzed utilizing the Worldwide Harmonised Light Vehicle Test Procedure (WLTP) brake cycle. Geometric mean diameters for both pads were found with a bimodal distribution in the ultrafine range. $PM_{10}$ emission factors of 15.1 ± 0.1 mg/km and 16.3 ± 0.4 mg/km were measured, which is 2.15 and 2.32 times higher than upcoming maximum permitted emission factor of 7 mg/km. On average 54.9 % and 58.1 % of PM10 was emitted as iron, with a wide variety of Fe concentrations between 43 – 75 % by mass found in individual particles. Other heavy metals, such as Cu, Cr, Mn and Zn, were also found and a high contribution of wear from the brake disc was noticeable, based on the elemental composition. Fe emission factors calculated from the WLTP brake cycle were 8–9 times higher than previously reported values in literature, while Cu levels were significantly lower based on recent trends in brake pad formulations. Four different PAH were detected even at the relatively low temperatures that are common for the WLTP brake test cycle.

## 1. Introduction

Automotive emissions derived from combustion engines have long been the focus of many researchers worldwide and underwent significant reduction due to regulatory measures by governments in the last decades [1]. However, non- exhaust emissions have long been disregarded in this discussion, even though they contribute a large fraction to traffic emissions. It is estimated that in the year 2016 non-exhaust emissions made up 73 % of traffic derived $PM_{10}$ emissions [2], with brake emissions contributing between 16 to 55 % of non-exhaust emissions, heavily depending on the braking frequency of vehicles at the studied location [3]. For these reasons, non-exhaust emissions (NEE) from automotive traffic have gained increasing attention, which is reflected by the fact that the upcoming EURO 7 norm will define maximum emission factors for particles originating from brakes and tires for the first time [4]. Furthermore, many studies are dealing with their toxicological impact and human health risks without a consensus on consistent setups [2]. Indeed, comparability of these studies has been lacking due to the huge differences in the used test setups, which range from pin-on-disc tribometers, to brake dynamometers with various designs, to "real-world driving scenarios" and environmental studies ([5]; Mathissen et al., 2019). For this reason, the particle measurement programme (PMP) of the United Nations Economic Commission for Europe (UNECE) has developed the United Nations Global Technical Regulation No. 24 (GTR24) for more comparable brake emission measurements, utilizing a uniform test cycle in the form of the Worldwide Harmonized Light Vehicle Test Procedure (WLTP) brake cycle, as well as a strict measurements procedure with defined maximum allowed deviations for speed, temperature and a range of other relevant parameters. The brake temperature plays a crucial role in emission testing [5], which is why applied vehicle parameters, like the weight of the brake disc in comparison to the vehicle weight are very important. This is accounted for by the GTR 24 via the implementation of four different groups of wheel load to disc mass ratios, which each have a different target range of the brake temperature. Such measures facilitate a more controlled testing procedure, which greatly enhance the comparability of studies. Type approval on GTR24 compliant brake dynamometers will be mandatory starting from 2026, with the EURO 7 norm defining maximum allowed $PM_{10}$ emission factors of 3 mg/km for pure electric vehicles, 7 mg/km for internal combustion engines and hybrid cars, as well as 11 mg/km for internal combustion engine vans. These emission factors will be further lowered to 3 mg/km for all light-duty vehicles in 2035 [6].

Common brake pad formulations, such as so called low metallic (LM) pads often contain metal contents around 10 – 30% of mass, while the softer non-asbestos organic (NAO) pads generally contain lower amounts of metals [7]. Additional differences in brake pad formulations arise from local legal regulations, most prominently the EPA's Memorandum of Understanding on Copper Mitigation in Watershed and Waterways [8], which limits the amounts of asbestiform fibers, chromium(VI)-salts, mercury and lead to 0.1%, cadmium compounds to 0.01% and copper to 5% of weight from 2021, with further restrictions that allow a maximum amount of copper of 0.5% starting in 2025. The usage of different friction pairings with varying brake pads and brake discs, influences the emission behavior of a brake system. For example, NAO pads normally release less PM, however they facilitate a higher wear of the brake disc, due to higher contents of abrasive fibers [5].

The need for legal restrictions of heavy metal concentrations originating from brake wear, as well as the demand to monitor compliance with such regulations is supported by literature, which lists brake wear as major contributor to ambient particulate Cu levels. A study conducted within "The Brake Pad Partnership" estimated emission factors for the nine sub-watersheds in the San Francisco bay area of 53.8 tonnes of Cu/year as airborne emissions, plus an additional 50.4 tonnes of Cu/year released to roadways [9], while a study from Hulskotte estimated that 2.4 kilotons of Cu are deposited to surface waters annually and that up to 75% of the atmospheric copper input in the North Sea may be due to brake wear [10].

Particles formed via abrasion of brake discs and pads have been found to be a potential threat, not only to the environment, but also to human health, since they contain high amounts of heavy metals such as Fe and Cu, a variety of other heavy metals, and minerals like anatase or graphite [11,12]. Airborne copper particles entering the human respiratory system, are expected to be toxic, with studies particularly pointing out the cytotoxic effects of copper nanoparticles in human alveolar models [13], while iron rich particles are often falsely disregarded as innocuous. This assumption is based on the fact that the human body has numerous pathways of dealing with large contents of Fe, preventing the generation of ROS by chelating the unbound iron if digested orally (Morgan et al., 2020), however, the lung does not possess pathways of dealing with large amounts of unliganded iron species (Ghio et al., 2009). Several studies have shown severe health impacts following inhalation of iron rich particles, particularly from PM mixtures containing reduced and oxidized iron (Beck-Speier et al., 2009; Lay et al., 1999; O'Day et al., 2022). The carcinogenic potential of long-term exposure to low-dose $Fe_2O_3$ nanoparticles resulting in neoplastic-like transformation of human small airway epithelial cells via formation of ROS was reported, as well as the potential neurotoxic and cardiovascular effects of iron-rich PM [14-16]. The chemical composition of brake-abrasion particles is thus related to their toxicological potential and their ability to induce oxidative stress, pro-inflammatory responses and DNA damage resulting in concerns for the human health [17]. For instance, increasing metal content of brake wear particles also increased tight junction damage, thus possibly decreasing lung epithelial barrier functions via intracellular formation of reactive oxygen species [18]. Abrasion derived particles are known to exhibit different toxicological responses compared to combustion derived Fe particles, often due to

rough and flake like shapes (Morgan et al., 2020). Studies on the toxicity of subway aerosol, which is similar in its chemical and morphological properties (Bendl et al., 2023) have revealed increased cytotoxicity and a twofold increase in DNA damage compared to $Fe_2O_3$ or $Fe_3O_4$ particles, attributed to the increased and highly active surface of these particles (Karlsson et al., 2006; Loxham and Nieuwenhuijsen, 2019). Furthermore, while ambient concentrations of low-metallic brake pad formulations did not induce biological responses in a multicellular in vitro model of lung, the presence of anatase in non-asbestos formula was associated with decreased cell viability and pro-inflammatory activity following pseudo-air-liquid-interface exposures [11].

While the EURO 7 regulation focusses on $PM_{10}$ emission values, smaller particles can also be generated during the braking process. Garg et al. reported the fraction of ultrafine particles of up to 33% of the airborne PM [19], which are not addressed in the EURO 7 legislation. Smaller particle sizes are of special concern, since the PM2.5 fraction is able to penetrate deep into the lungs and particles smaller than 0.1 μm can even deposit in the alveoli, from where they eventually reach the bloodstream via the blood-air barrier [20]. Metal containing nanoparticles are reportedly also able to penetrate to the central nervous system via the nasal route, followed by uptake and transport in the olfactory nerve [21,22].

Apart from heavy metals and minerals, brake wear emissions can emit other known pollutants, such as polycyclic aromatic hydrocarbons (PAH) and other harmful organic compounds, formed via thermal degradation of organic substances. The high local temperatures at the tribological interface of the brake can facilitate thermal degradation of the organic binding matrix, which is usually composed of modified phenol-formaldehyde resins [5]. Gasser et al. also reported an increased release of pro-inflammatory mediator interleukin-8 during strong braking, which they attributed to organic compounds and black carbon [18]. So far little is known on the organic emissions of brake wear and only a few studies have investigated this topic [23].

Due to the metallic nature of brake wear and the large differences in elemental composition in different brake lining types, not only the generated particle mass and numbers, but also the concentrations of heavy metals in particles is of utmost importance to assess the potential health threats of a specific pad. For this purpose, inductively coupled plasma tandem mass spectrometry (ICP-MS/MS) is a suitable technique for sensitive quantification of a large variety of elements in filter samples, as well as bulk brake lining material. Furthermore, the distribution of elements throughout different size ranges is important for the evaluation of potential health impairing effects. For this purpose, SEM/EDX analysis is a beneficial orthogonal technique for the detection of elements like Si and C that are not accessible by conventional ICP-MS/MS analysis, providing additional information about the distribution and homogeneity of brake wear markers over different size ranges.

The aim of this study was the comprehensive physical and elemental characterization of brake dust, emitted under standardized conditions, as close to those defined by the GTR24, providing a broader understanding of the chemical composition and the distribution of environmental and health impairing pollutants among different size ranges from coarse to ultrafine. To our knowledge this is the first in-depth characterization of brake dust on a modern dynamometer design exceeding the scope of measurements defined within the GTR24.

## 2. Methods and Materials

### 2.1. Brake dyno setup and test cycle procedure

Brake wear measurements were conducted utilizing a custom-built brake dyno (manufacturers: AiP automotive for construction and design; HDC Blueprints for Project management, automatization, construction and operation) designed to fulfill the specifications in the GTR24 [24] by the PMP of the UNECE. All requirements for the design of the brake dyno, except for the orientation of the brake housing, which is located vertical instead of horizontal, and the symmetry of the housing, which is slightly asymmetrical at the exit point. A constant volume sampler (CVS) was utilized to maintain a consistent cooling air flow throughout emission tests and isokinetic nozzles were installed in front of all sampling probes. Images of the brake dyno and its compartments are depicted in Fig. 1.

Original 330 mm by 24 mm brake discs, as well as a brake caliper fitting a 17-inch tire rim, were supplied by the original equipment manufacturer (OEM) of the simulated vehicle and were utilized for all measurements. The specifications for the simulated vehicle can be found in Table S1 in the supplementary information (SI). Whenever new brake pads were installed, brake discs were also changed to new discs. LM brake pads were directly supplied by the OEM and were tested together with commercially available NAO pads from the aftermarket. Thermoelements for monitoring brake disc temperatures were embedded according to the GTR24 with data being obtained with 10 Hz resolution. The WLTP brake cycle, comprising 303 individual brake events, was utilized for brake emission tests.

As required by the GTR24 a minimum of five WLTP brake cycles were conducted for the bedding of newly installed brake discs and pads before testing. The cooling air flow of the system was adjusted according to the GTR24, by determining the wheel load to disc mass ratio and measuring the corresponding temperatures during Trip #10 of the WLTP brake. Results from the cooling air speed adjustment, as well as the specific values for the simulated vehicle requested by the GTR24 are listed in Table S2 in the SI, while the brake disc temperatures during the WLTP brake cycle are plotted in Fig. S1 in the SI. Based on these results the CVS was set to a flow rate of 540 $m^3$/h for the LM pad and 720 $m^3$/h for the NAO pad.

### 2.2. Online measurements, gravimetry & filter sampling

The measurement setup for the determination of brake wear emissions and toxicity is illustrated in Fig. 2. All measurements required by the GTR24, except for the total particle counter (TPC), were conducted in the brake test cell, whereas all additional instruments were located in the control room outside of the test cell and were connected via two 12 mm outer diameter stainless steel tubes, depicted as green & red lines in Fig. 2.

A condensation particle counter (CPC) (SPC-D-19, AiP automotive), equipped with a catalytic stripper and a built-in dilution system, with a dilution factor of 1:100, acted as solid particle counter (SPC).

The green line was diluted 1:25 via a portable dilution system (Dekati eDiluter Pro, Dekati Ltd.), providing suitable particle concentrations for the downstream instrumentation. Clean air for dilution was supplied via a zero-air generator (AADCO 737–15, Tisch Environmental Inc.) to avoid contamination and influence on measurements results. A second CPC (Grimm 5420, Grimm Aerosol Technik GmbH & Co. KG,) was utilized as TPC and additional filter sampling for chemical analysis was conducted via a gravimetric filter holder (Dekati eFilter, Dekati Ltd.). Particle size-distributions in the range of 0.3 – 2.5 μm were measured with a resolution of 0.5 Hz via an Optical Particle Sizer (OPS) (Aerosol Particle Size Spectrometer LAP 322, Topas GmbH),

The red line was connected without any dilution to a Fast Aerosol Sizer (DMS500 Mk II, Cambustion Ltd.), measuring size distributions in the range of 5 nm – 1 μm with a resolution of 1 Hz.

Samples were drawn on a variety of filter materials. PTFE membrane filter discs with a diameter of 47 mm (Teflo 2 μm, 47 mm, Pall Corporation) were used for gravimetric measurements and ICP-MS analysis and were loaded in the $PM_{10}$ and $PM_{2.5}$ filter holders, installed in the brake test cell. The Dekati eFilter was set to a flow of 10 L/min for sampling on 47 mm quartz fibre filters (Whatman QMA 47 mm, Cytiva), which were used for analysis of PAHs and 47 mm polycarbonate (PC) track-etched filters (Whatman, Nucleopore, 2 μm pore-size) for SEM/EDX analysis. For SEM/EDX analysis silica wafers (p-type boron dotted 5 ×5 mm, Ted Pella Inc.) and pure Nb substrates (EM-Tec NB12, ø


**Fig. 1.** Images from the initial installation of the custom-built brake dyno for emission measurements. 1. Brake enclosure 2. Sampling point, filter holder location and closet housing the SPC 3. CVS system.

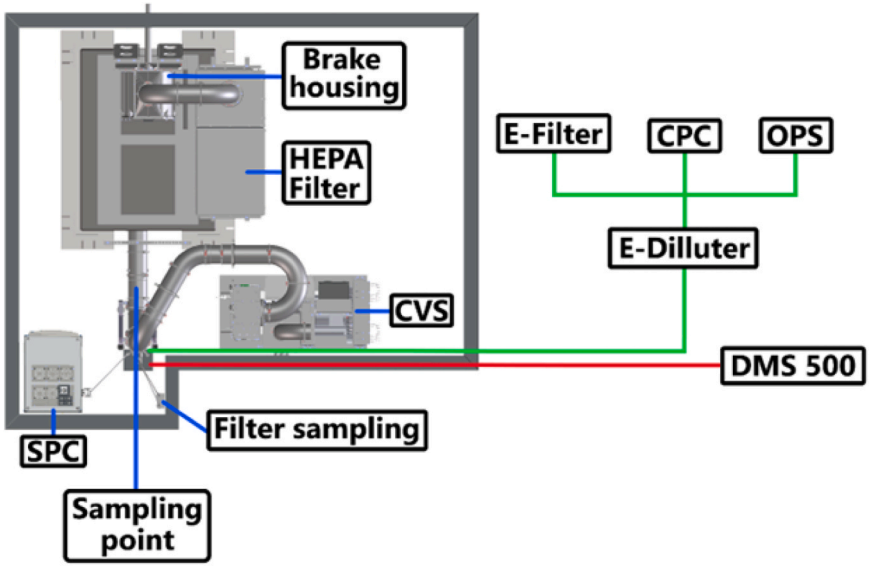


**Fig. 2.** Setup for the brake wear measurement campaign (top view). Sampling line 1 (green) was equipped with a $PM_{2.5}$ cyclone at the inlet, while sampling line 2 (red) was equipped with a $PM_{10}$ cyclone, followed by a $PM_1$ cyclone for the DMS500. All instruments on the green line were diluted 1:25 by the E-Diluter. The DMS500 connected to the red line measured undiluted.

12 ×0.1 mm, 99.99 % Nb, Micro to Nano) were placed on top of the filters. These additionally sampled substrates were used for a variety of benefits giving a holistic overview of the sample. Silica wafers show a smooth, polished surface and excellent conductivity, offering a good substrate for high-resolution micrographs, excelling in the analysis of nanoparticles, while Nb plates are a more suitable medium for EDX analysis of small particles, where a portion of the electron beam can pierce the particles and excite x-ray transitions from the underlying substrate, falsifying the data. Both sample types potentially suffer from being a passive sampling approach, therefore being prone to altered size distributions of sampled particles. PC filters were also analyzed to compare particles found on Si wafers and Nb plates to an unaltered size distribution, ensuring a representative analysis. All analysed filters of the same type originated from the same batch. At least three blank filters were analysed for every filter type with each measurement technique.

Gravimetry was carried out by weighing filters before and after each WLTP brake cycle, using a micro-balance (Cubis MCA2.7S-2S00-F, Sartorius). Before each weighing filters were pre-conditioned at a relative humidity of 45 % and a temperature of 22 °C for 24 h in a climate-controlled chamber (pureGMC 18-EPA1065), equipped with a corona discharger for filter charge neutralization.

### 2.3. ICP-MS/MS analysis

Bulk material analysis of both brake pads, as well as the brake disc were carried out by grinding powder samples from the top layer of new pads. A tungsten carbide grinder was utilized to generate these powders, to avoid possible contamination with iron and other metals originating from the tools.

Loaded PTFE filters and powder samples were digested with a microwave assisted pressure digestion according to the VDI regulation 2267 [25] by placing the samples in PTFE vessels and adding 8 ml of 69 % $HNO_3$ (Rotipuran Supra, Carl Roth GmbH + Co. KG), followed by 2 ml of $H_2O_2$ (Rotipuran, Carl Roth GmbH + Co. KG),) and 10 µl of a mixed internal standard solution (100 µg/ml Bi, Ge, In, $^4$Li, Lu, Rh, Sc, Tb, Agilent Technologies). Sealed samples were then heated in a ventilated microwave (MARS 5, CEM) following a pre-defined temperature gradient for 180 min. Before the analysis samples were diluted to a final volume of 50 ml with Millipore water (18.2 MΩ·cm at 25 °C) and filtered with syringe filters (Whatman Puradisc, pore size 0.2 µm, Cytiva).

Analysis was conducted with an Agilent 8900 triple quadrupole ICP-MS/MS. During the analysis a constant volume of an Yttrium standard

solution (High-Purity Standards) with a concentration of 0.5 mg/L was added via a peristaltic pump and a T-piece, to assess the signal drift and plasma stability. The utilized reaction gases and measured *m/z* values for ICP-MS/MS analysis are listed in Table S3 in the SI.

### 2.4. SEM/EDX analysis

SEM/EDX analysis of bulk brake wear linings was carried out by cutting small samples of approximately 5 × 10×5 mm from the friction surface of each pad. Prior to sampling the bedding process of 5 WLTP brake cycles was carried out to remove the brake in coating present on the NAO sample and to obtain a representative sample for a bedded brake pad.

Samples with a diameter of 12 mm were cut from PC filters and were transferred to SEM pin stubs with conductive high purity EDX suitable double-sided carbon adhesive pads in-between (Spectro-Tabs, Plano GmbH). Silica wafers and Niobium plates were secured to SEM pin stubs with conductive silver paint (EM-Tec AG15, Micro to Nano). Samples were then stored in a desiccator under vacuum for at least 24 h to ensure removal of volatile components hindering analysis. Wafer and Nb plate samples were left unaltered, while filter samples were coated with a thin carbon layer of approximately 10 nm, to minimize charging effects during analysis. A Q150T ES Plus sputter device (Quorum technologies) with a woven carbon fiber string (density 1.55 g/m, Quorum technologies) was used in pulsed cord evaporation mode for the application of a conductive carbon layer of approximately 10 nm.

SEM micrographs were taken with the Inlens and SE2 detectors of a Gemini Sem 360 (Carl Zeiss) field emission SEM at acceleration voltages of 0.75 – 1.5 kV. EDX analysis was conducted with an Ultim Max 40 EDX detector (Oxford Instruments) equipped with a thin polymer detector window and a Silicon drift detector, granting the ability to measure low-Z elements (Z > 6). EDX analysis of particles with a geometric diameter > 200 nm was carried out with an acceleration voltage of 12 kV, while particles smaller than 200 nm were analysed with 5 kV, to minimize piercing of the electron beam through the particles. The chosen acceleration voltages were based on simulations of electron penetration depths and X-ray excitation responses of particles in the Monte Carlo Casino software, as demonstrated in a previous study on brake- and rail wear particles emitted by subway trains [26].

At least 25 particles were measured for each filter and substrate type and in total more than 100 particles were analyzed for each brake pad.

### 2.5. GC-MS/MS analysis

From each quartz fiber filter five punches with a diameter of 8 mm were cut and extracted with 980 µl of acetone and 20 µl of a 5 µg/ml internal standard solution (PAH Analyzer Calibration Sample Kit, Agilent) containing five deuterated PAHs, in an ultrasonic bath for 60 min. Before analysis samples were filtered with PVDF syringe filters with a 0.2 µm pore size (Rotilabo®, Carl Roth) to remove particles prior to the injection into the system.

Filter extracts were measured for 27 different particle bound PAHs via an Agilent 8890/7000D triple quadrupole GC-MS/MS PAH analyzer with $H_2$ as carrier gas and an Agilent DB-EUPAH, 20 m × 0.18 mm, 0.14 µm column following the application note 5994–2192EN by the manufacturer [27]. An average recovery rate of 79.7 % was calculated for 12 PAHs by extraction of a certified reference material (ERM-CZ100 – Fine dust PM10-like, Joint Research Centre of the European Commission). The individual recovery rates for the individual PAHs are listed in Table S4 in the SI. Final PAH concentrations were obtained by correcting the measured concentrations for each PAH in the extracts with the corresponding recovery rate if applicable and with the average recovery rate for those where no value was available.

## 3. Results and discussion

### 3.1. Online measurements & gravimetric analysis

The averaged PM emission factors for three runs at the brake and vehicle level conducted with LM and NAO brake pads are listed in Table 1. PM data of the tested single front brake was multiplied with the volumetric flow of the CVS and was divided by the sampling air flow of the filters. The obtained total PM emissions during the WLTP brake cycle were then divided by a factor of 192, which is the total driven distance during the cycle in km, to obtain single front brake emission factors. The formula used for calculating emission factors (EF) of the front brake is given in Eq. 1.

$$EF_{front\ brake} = \frac{Flow_{CVS}}{Flow_{Filters}} * \frac{PM}{192\ km} \quad (1)$$

Vehicle level emission factors were calculated from emission factors (EF) of the single front brake following Eq. 2, which is adopted from the GTR 24. A standard brake force distribution (FAF) between front and rear axle with a share of the braking force applied to the front axle of 66 % of the total braking force was utilized, which is also the normal distribution of the simulated vehicle. The FAF is further multiplied by a factor of 0.5, since the brake force on the front axle is shared between the two front brakes. A friction braking share coefficient (c) of 1.0 was applied, which refers to the amount of electric recuperation in the deceleration of the vehicle, which is 1.0 per definition for vehicles with only an internal combustion engine.

$$EF_{vehicle} = \frac{EF_{front\ brake}}{FAF * 0.5} * c \quad (2)$$

The LM pad emission factors at the vehicle level were found at 15.1 ± 0.1 mg/km of $PM_{10}$, which is 2.2 times higher than upcoming maximum permitted emission factor of 7 mg/km, while the NAO pad was 2.3 times higher than permitted from 2026 onwards, with a $PM_{10}$ emission factor of 16.3 ± 0.4. The OEM LM pad showed single brake emission factors of 5.0 ± 0.1 mg/km for $PM_{10}$ and of 1.8 ± 0.0 mg/km for $PM_{2.5}$. These values are well comparable to the most recent global interlaboratory study (ILS II), which reported average emission factors of 5.0 mg/km for $PM_{10}$ and 1.9 mg/km for $PM_{2.5}$ with the friction pairing ILS II brake 1 with pad a (BR1Fa) with a LM pad and a slight lighter simulated vehicle weight of 1600 kg [28]. However, when comparing the average single brake emission factors of the aftermarket NAO pad, which was measured at 5.4 ± 0.1 mg/km of $PM_{10}$ and 2.4 ± 0.1 mg/km of $PM_{2.5}$, to the values reported for the ILS II brake 1 with brake pad b (Br1Fb), which is the same vehicle as Br1Fa, but equipped with a NAO pad, emissions were significantly higher. For NAO pads Grigoratos et al. [28] reported an average of 2.2 mg/km of $PM_{10}$ and 0.8 mg/km of $PM_{2.5}$, which is only 40.5 % of $PM_{10}$ and 33.2 % of $PM_{2.5}$ found in this study. The ILS-II was chosen as reference point for PM and PN data, since it was the only study with a GTR compliant brake dynamometer at the time of this study. The Br1Fa and Br1Fb friction

**Table 1**
PN and PM emission factors of LM and NAO brake pads on the brake and vehicle level.

| Brake pad | Emission level | TPN #/km | SPN #/km | $PM_{10}$ mg/km | $PM_{2.5}$ mg/km |
|---|---|---|---|---|---|
| LM | Single front brake | 4.51 ± 0.06 × $10^9$ | 5.49 ± 0.11 × $10^9$ | 5.0 ± 0.1 | 1.8 ± 0.0 |
| | Vehicle | 1.37 ± 0.02 × $10^{10}$ | 1.65 ± 0.03 × $10^{10}$ | 15.1 ± 0.1 | 5.4 ± 0.1 |
| NAO | Single front brake | 8.26 ± 0.1 × $10^9$ | 8.50 ± 0.21 × $10^9$ | 5.4 ± 0.1 | 2.4 ± 0.1 |
| | Vehicle | 2.50 ± 0.03 × $10^{10}$ | 2.55 ± 0.06 × $10^{10}$ | 16.3 ± 0.4 | 7.2 ± 0.2 |

pairings were deemed the most comparable, due to used vehicle weight and availability of data for both LM ad NAO pads. Observed differences can be partially attributed to differences in the simulated vehicle, wheel load to disc mass ratios and utilized friction pairing, the most likely explanation is the high metal content that was measured in the NAO brake lining of 15.8 %, which is unusual for such pad formulations (for further discussion see chapter 3.2 ICP-MS/MS analysis in the results section). When comparing the aftermarket NAO pads emission factors to those of an LM pad, which from the chemical characterization of the bulk brake lining material appears to be a more suitable classification for the pad, the results are again in a similar range compared to the ILS II. The obtained emission factors resulted in average $PM_{2.5}/PM_{10}$ ratios of 0.36 for the LM and 0.44 for the NAO pad, which is lower for the LM pad than the values of 0.42 to 0.45 reported by the ILS II. Since the temperature has a large influence on the emitted particle size [5], with higher temperatures resulting in smaller particles, the lower values for the LM pad are to be expected when comparing to the BR1Fa with a 10 °C higher required average braking temperature based on differences in wheel load to disc mass ratio. The NAO pad also reached a slightly higher maximum temperature of 122 °C, compared to 114.6 °C of the LM pad, which could explain the shift in emissions towards smaller particles.

The measured total particle number (TPN) and solid particle number (SPN) emissions averaged over three runs for the LM and the NAO pad are listed in Table 1 and the average measured particle #/cm$^3$ for individual WLTP brake cycles, measured by the SPC are given in Table S5 in the SI. PN emissions from the LM pad were 2.3 (TPN) and 2.5 (SPN) times higher than values of the ILS II, which reported a TPN of $1.93 \times 10^9$ #/km/brake and a SPN $2.19 \times 10^9$ #/km/brake on average [29]. For the NAO pad the emission were 8.8 (TPN) and 8.3 (SPN) higher than the ILS II that measured $9.37 \times 10^8$ #/km/brake (TPN) and $1.03 \times 10^9$ #/km/brake (SPN) for the BR1Fb. However, as discussed for the PM values, the NAO pad can be better compared to the ILS BR1Fa due to its high metal content, which would result in 4.3 (TPN) and 3.9 (SPN) times higher PN emissions. Since numerous variables, such as brake temperature, formulation of the brake pad, the wheel to disc mass ratio and the weight of the simulated vehicle have a strong impact on emitted particle sizes and numbers [12], it is difficult to compare PN data of two different configurations, with different vehicles, friction pairings and dynos. This is also reflected by the high range of TPN reported by the ILS II, which ranged from $9.1 \times 10^8$ #/km/brake to $1.1 \times 10^{10}$ #/km/brake for the 7 tested brakes.

In general, it can be concluded that the used brake dyno setup, albeit minimally deviating from GTR24, yielded feasible emission factors, suitable for physical and chemical investigations.

The time resolved TPN concentrations measured with a CPC are plotted against the speed profile of the WLTP brake in Fig. 3, showcasing the high impact of strong braking events and rapid successions of medium brake events on PN emissions. As visible in the graph, braking events resulted in distinct peaks, well distinguishable from the background noise even for weaker braking events.

The DMS 500 revealed similar bimodal PN size distributions for both pads. The geometric mean diameter (GMD) for the LM pad was 123 nm, while the NAO pad had a GMD of 143 nm. Both pads showed a second mode around 86 nm, which was more distinct for the NAO pad. This is in good agreement with several published studies, which reported peaks for the particle number around 70 to 100 nm [30-32]. The OPS showed the optical mode between 300 and 400 nm, with PN levels steeply declining above the 400 nm mark. The OPS, in contrast to the DMS 500, measured more particles in the size bin around 400 nm than around 300 nm, which is likely caused by the lower counting efficiency of OPS instruments for smaller particles [33]. Up to particle sizes of 500 nm the DMS 500 data can be regarded as more accurate, due to the measurement principle being based on the electric mobility of particles, instead of their light scattering properties. PN size distributions for LM and NAO pads obtained by DMS 500 and OPS are shown in Fig. 4. The NAO pad produced a larger share of smaller particles compared to the LM pad, visible from the data obtained from the DMS 500, while the OPS showed no equal increase in large particles. This is also reflected by the higher $PM_{2.5}/PM_{10}$ ratio and the higher TPN and SPN values for the NAO pad, since small particles often have a large influence on PN, however, a negligible influence on PM. Overall the majority of particles was distributed between 40 and 300 nm, with a considerable fraction in the ultrafine region, and the GMD slightly above the ultrafine region. Some

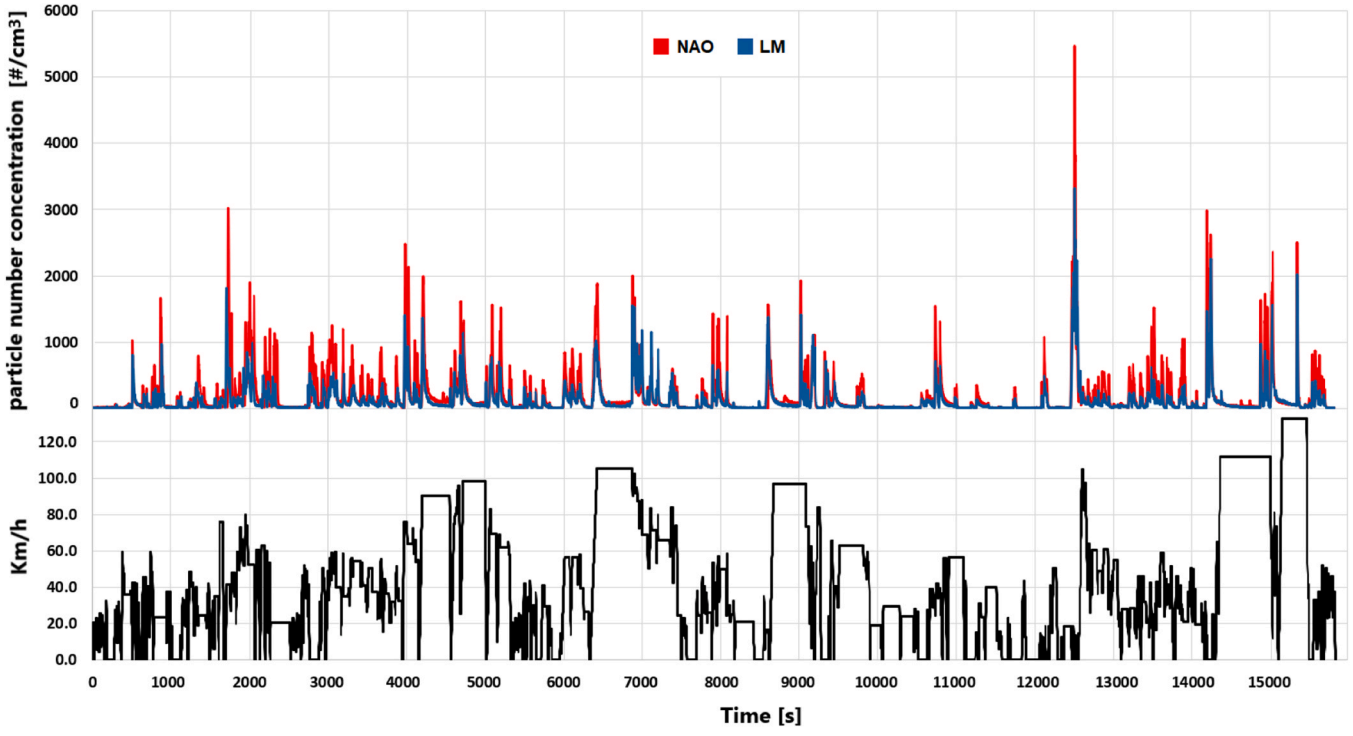


**Fig. 3.** TPN emissions of LM & NAO pads plotted against the WLTP brake speed profile.

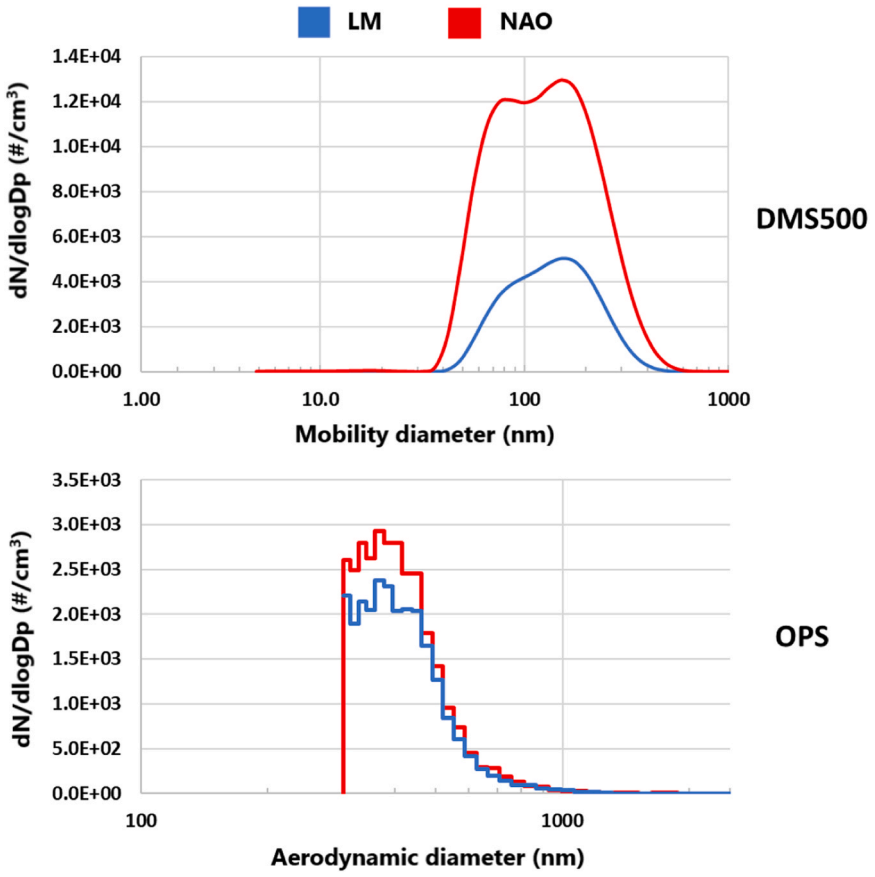


**Fig. 4.** Size distributions for LM & NAO pads averaged over the WLTP brake cycle measured via DMS500 (5–1000 nm) and OPS (300–2500 nm).

studies also reported smaller particles between 10 nm and 30 nm for strong braking events [30], which are linked to a critical temperature of the brake [12], where local temperatures at the friction interface are high enough to melt iron, leading to condensation of ultrafine particles in the cooling air stream [19]. Garg et al. further reported that 33 % of $PM_{10}$ are emitted as ultrafine particles [19], showcasing the high abundance of small particles, which is in good agreement with results from this study. Since future amendments to the EURO 7 will feature maximum PN emission factors from 2030 onwards [4], such findings are not only critical regarding human health, but pose a large challenge to manufacturers, as ultrafine contribute greatly to PN emissions.

### 3.2. *ICP-MS/MS analysis*

The ICP-MS/MS analysis of bulk brake wear material and particles emitted during brake events, showed a significant difference in chemical composition for both brake pads. While the LM brake lining bulk material contained 23.9 ± 0.4 wt% of Fe, the particles in $PM_{10}$ samples emitted by the LM pad averaged at 54.85 ± 0.85 wt%. The higher Fe content in filter samples can be explained by the fact that emitted particles are not solely originating from the brake pad, but are a mixture of wear from brake pad and brake disc. The Fe content of the utilized brake disc was measured at 81.8 ± 2.4 wt%, accounting for the elevated iron contents in the mixture of particles. This hypothesis is further supported by other heavy metal concentrations, such as Mn which increased from 0.1 ± 0.0 wt% in the LM bulk material to 0.29 ± 0.0 wt% in the filters, while the brake disc contained an average of 0.56 ± 0.01 wt% of Mn. The same shift in heavy metal concentrations was also observed in the opposite direction for several elements e.g. Cu, where the LM bulk material contained 0.50 ± 0.04 wt% of Cu, whereas the $PM_{10}$ filter samples contained 0.29 ± 0.00 wt% of Cu and the brake disc only 0.28 ± 0.01 wt% of Cu. This trend is most noticeable for Zn concentrations, which lowered from 5.57 ± 0.20 % in the brake lining material to 1.46 ± 0.03 % in $PM_{10}$ samples, most likely due to the absence of Zn in the brake disc, which contained only 0.03 ± 0.02 %. Such changes in elemental composition from the initial brake lining material to the emitted particles are well reported in literature and can not only be attributed to the abrasive wear of the brake disc, but also to a variety of other parameters, such as speed, severity and frequency of braking events and individual driving and braking behaviour [12,34]. Kukutschová listed the lower melting points of the common brake marker elements Cu, Zn and Sn compared to Fe as possible source for enrichment of mentioned metals in nanoparticles [12], while Österle proposed that local temperatures at the friction interface are high enough to cause thermal degradation, or even evaporation of the organic material [35], which would also account for elemental changes originating from the braking process.

ICP-MS/MS analysis of the NAO bulk material revealed average Fe contents of 13.9 ± 1.1 wt%. Such concentrations are unusually high for such a pad formulation and fit rather into the category of an LM pad, which generally contain between 10 - 30 % of Fe [7]. This result can also explain the high PM and PN emission factors found for this pad, since emission values of this pad were well in accordance with those of a LM pad formulation. The ICP-MS/MS results of the analyzed NAO pad showed, that manufacturers classifications of the brake pad types, which in most parts of the world is neither mandatory, nor regulated regarding their chemical composition, is not always sufficient to estimate the emission behavior of a certain brake pad.

Elemental compositions of $PM_{10}$ filter samples showed an increased Fe content of 58.1 ± 1.4 %, which was even higher than the Fe content found in the LM samples, suggesting an increased wear of the brake disc. A high contribution of disc wear to the sampled particles is also

supported by the Cu contents measured in $PM_{10}$ and $PM_{2.5}$ samples. The original brake lining material measured almost no copper, showing the impact of US EPAs restriction of copper usage in brake pads, while the emitted particles contained on average 0.21 ± 0.01 % ($PM_{10}$) and 0.20 ± 0.01 % ($PM_{2.5}$) of Cu.

Elemental compositions of the bulk brake lining material were similar to those found by Kukutschová, however, Cu concentrations were significantly lower than the reported 7.7 %, which can be attributed to changes in modern pads based on the ban on copper in the U.S [12].

Elemental compositions of $PM_{10}$ and $PM_{2.5}$ filter samples for each pad were very similar showing an even distribution of elements over the coarse and fine size region. However, for Sn an enrichment in the $PM_{2.5}$ fraction of the LM pad was observed with 0.78 ± 0.05 wt% of Sn in the $PM_{10}$ fraction and 1.03 ± 0.01 wt% in the $PM_{2.5}$ fraction. The effect was not present for the NAO pad, however, Sn concentrations were much lower than in the LM pad. Kukutschová et al. attributed the enrichment of certain elements such as Cu, Zn and Sn to the comparably low melting points of these metals, facilitating their potential to form nanoparticles at elevated temperatures [12]. This effect was only observable for Sn, which has an especially low melting point of 232 °C, which is plausible considering the generally low temperatures during the WLTP brake cycle. A second effect that was only noticeable for the LM pad was the enrichment of Cr. While the brake pad initially contained 0.37 ± 0.02 wt% and the brake disc 0.22 ± 0.01 wt% of Cr, the $PM_{10}$ and $PM_{2.5}$ filters showed concentrations of 0.61 ± 0.01 wt% and 0.60 ± 0.01 wt% respectively. A general trend that was also observed, was the reduction in chemical differences in the composition of emitted particles for both $PM_{10}$ and $PM_{2.5}$ in LM and NAO samples, due to mixing with wear from the brake disc, which was the same for both pads.

Fig. 5 illustrates the elemental changes from bulk materials to $PM_{10}$ samples caused by the contribution of brake disc wear. The numerical values for chemical compositions of initial brake lining materials, as well as the cast iron brake disc measured via ICP-MS/MS, are listed in Table 2, while the chemical compositions in $PM_{10}$ and $PM_{2.5}$ samples are given in Table 3.

Average emission factors for heavy metals were calculated from the gravimetric and ICP-MS/MS results and are plotted in Fig. 6, and the numerical values are listed in Table S6 in the SI. On average the $PM_{10}$ emission factors of the LM pad were 8.3 ± 0.1 mg/km of Fe and 44.9 ± 0.3 µg/km of Cu, while the NAO pad exhibited emission factors of 9.5 ± 0.2 mg/km for Fe and 33.6 ± 1.1 µg/km of Cu. A literature review by Grigoratos and Martini summarized the emission factors for heavy metals reported in several studies and found Fe emission factors of up to 1 mg/km for light duty vehicles and Cu emission from 50 to 700 µg/km [5]. Results from this study were substantially higher than Fe emission factors reported in the literature review by Grigoratos and Martini, showing that the $PM_{10}$ emission factors of previously published studies still have to be put into context with modern dyno designs and GTR24 compliant measurements.

Especially high copper emission values are of concern, considering its massive accumulation in the environment [10] and human exposure to airborne copper particles. Therefore, it is a positive trend that copper contents of brake pads are globally declining, most likely due to the EPA regulations. This can be seen by the analysis of the bulk brake lining material, which showed the compliance of both pads to the current regulations and the NAO pad being almost completely copper free. As a result of these changes in brake pad formulations current Cu emissions from brake pads might be overestimated, based on results of older

**Table 2**
Elemental composition of brake bulk lining and brake disc material measured via ICP-MS/MS.

| Element wt% | LM Pad | NAO Pad | Brake disc |
|---|---|---|---|
| Fe | 23.9 ± 0.4 | 13.9 ± 1.0 | 81.8 ± 2.4 |
| Cu | 0.50 ± 0.04 | 0.01 ± 0.00 | 0.28 ± 0.01 |
| Cr | 0.37 ± 0.02 | 0.04 ± 0.00 | 0.22 ± 0.01 |
| Mn | 0.10 ± 0.00 | 0.07 ± 0.01 | 0.56 ± 0.01 |
| Al | 0.48 ± 0.03 | 1.56 ± 0.03 | 0.08 ± 0.02 |
| Zn | 5.57 ± 0.20 | 0.05 ± 0.02 | 0.03 ± 0.02 |
| Ba | 1.59 ± 0.02 | 0.02 ± 0.00 | 0.00 ± 0.00 |
| Mg | 4.12 ± 0.09 | 9.62 ± 0.08 | 0.01 ± 0.00 |
| Ni | 0.02 ± 0.00 | 0.01 ± 0.00 | 0.08 ± 0.00 |
| V | 0.01 ± 0.00 | 0.03 ± 0.00 | 0.01 ± 0.01 |
| Mo | 0.01 ± 0.00 | 0.00 ± 0.00 | 0.03 ± 0.00 |
| Sn | 2.86 ± 0.15 | 0.19 ± 0.04 | 0.08 ± 0.02 |
| S | 2.84 ± 0.30 | 2.31 ± 0.04 | 0.12 ± 0.01 |
| Total wt% of heavy metals | 33.8 ± 0.8 | 15.8 ± 1.2 | 83.2 ± 2.4 |

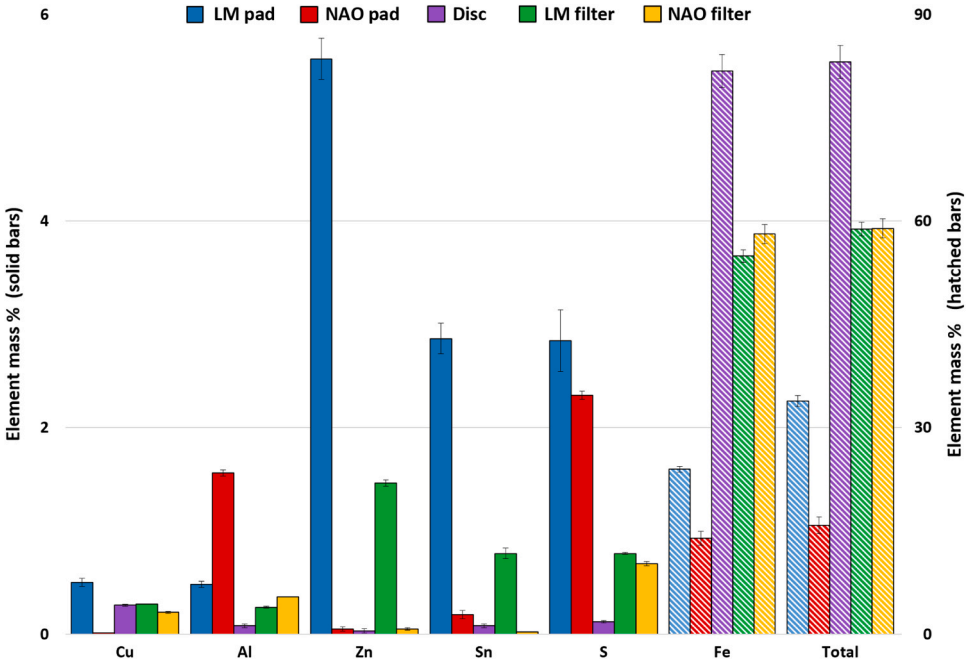


**Fig. 5.** Weight percentages for selected elements analyzed via ICP-MS/MS, illustrating the contribution of the brake disc to $PM_{10}$ samples. Solid bars are plotted on the left Y-Axis, while hatched bars are plotted on the right Y-Axis.

**Table 3**
Elemental composition of brake wear particles from LM and NAO filter samples analyzed via ICP-MS/MS.

| Element mass % | LM Pad | | NAO Pad | |
|---|---|---|---|---|
| | $PM_{10}$ | $PM_{2.5}$ | $PM_{10}$ | $PM_{2.5}$ |
| Fe | 54.9 ± 0.9 | 54.5 ± 1.2 | 58.1 ± 1.4 | 57.2 ± 1.8 |
| Cu | 0.29 ± 0.00 | 0.28 ± 0.00 | 0.21 ± 0.01 | 0.20 ± 0.01 |
| Cr | 0.61 ± 0.01 | 0.60 ± 0.01 | 0.13 ± 0.00 | 0.13 ± 0.00 |
| Mn | 0.29 ± 0.00 | 0.29 ± 0.00 | 0.31 ± 0.01 | 0.31 ± 0.01 |
| Al | 0.26 ± 0.01 | 0.24 ± 0.00 | 0.36 ± 0.00 | 0.28 ± 0.01 |
| Zn | 1.46 ± 0.03 | 1.45 ± 0.02 | 0.05 ± 0.01 | 0.01 ± 0.02 |
| Ba | 0.41 ± 0.01 | 0.40 ± 0.01 | 0.01 ± 0.00 | 0.00 ± 0.00 |
| Mg | 0.90 ± 0.04 | 0.90 ± 0.03 | 1.63 ± 0.02 | 1.72 ± 0.09 |
| Ni | 0.05 ± 0.00 | 0.05 ± 0.00 | 0.05 ± 0.00 | 0.05 ± 0.00 |
| V | 0.01 ± 0.00 | 0.01 ± 0.00 | 0.01 ± 0.00 | 0.01 ± 0.00 |
| Mo | 0.02 ± 0.00 | 0.02 ± 0.00 | 0.03 ± 0.00 | 0.03 ± 0.00 |
| Sn | 0.78 ± 0.05 | 1.03 ± 0.01 | 0.02 ± 0.00 | 0.02 ± 0.00 |
| S | 0.78 ± 0.01 | 0.78 ± 0.03 | 0.68 ± 0.02 | 0.71 ± 0.04 |
| Total % of heavy metals | 58.8 ± 1.0 | 58.6 ± 1.2 | 58.9 ± 1.4 | 58.0 ± 1.9 |

studies with other test setups and older brake linings types.

Fe rich particles are also reported to induce several adverse health effects following long-term inhalation [14-16]. This places further emphasis on the importance of the high PN of brake wear found in the submicron mode for both analyzed pads.

Additionally, brake dust is normally mixed with other heavy metals, such as Cu, Mn, Cr, Sn and V, complicating the assessment of the toxicological impact of such particles. Here especially the high Cr [36] and Zn [37] contents found in the LM pad, together with the higher percentages of Cu are of concern.

### 3.3. SEM/EDX analysis

SEM/EDX analysis of bulk material cut-outs showed a high inhomogeneity of the elemental distribution in both samples. The NAO pad displayed a more uniform distribution of iron throughout the sample, while the LM sample showed large flakes of iron. Furthermore, the NAO pad showed a higher abundance of steel fibres, which explains the more pronounced influence of brake disc wear on the chemical profile of emitted particles observed with ICP-MS/MS, since the addition of higher amounts of these fibres tends to increase rotor wear [38]. Primary plateaus, consisting of wear resistant compounds in the pad such as steel fibers and secondary plateaus, formed from compacted debris, were visible in both samples as part of the generated tribolayer [39,40]. Chemical mappings of LM and NAO bulk material cut-outs, with visible Fe flakes for the LM pad and a steel fibers in the NAO sample are shown in Fig. 7.

SEM micrographs of brake wear showed rough edged, splintery particles, typical for abrasion processes, which were found in all samples of both brake pads. Two main types of morphology, spherical and flake like particles, were commonly found throughout all samples. Flake like particles, shown with a yellow size marker in Fig. 8, were mainly found for particles > 1 µm, while spherical shaped particles, depicted in green, where found among all sizes. The images in Fig. 8 show particles from a LM sample, however, both pad types frequently displayed the two morphologies. Wahlström et al. attributed the flake like particle morphology to wear from the brake disc due to the absence of typical brake markers, such as Ti, Cu and Al [41]. However, SEM/EDX analysis also revealed flakes showcasing high concentrations of brake markers, such as Zn, which were not present in the bulk ICP-MS/MS analysis of the brake disc. Instead flake like particles exhibited similar chemical compositions as spherical particles.

EDX measurements showed high Fe contents in almost all particles, ranging between 43 % and 75 %. Two elements, C and O, were also found at high concentrations in all particles, with O ranging from 19 - 39 % and C from 2.5 - 32 %. An overview of morphologies and elemental compositions of NAO particles is given in Fig. 9, while a more detailed micrograph and elemental composition derived from the EDX spectra for a LM particle is presented in Fig. 10. Overall ranges of elements in particles were large, and no changes were observed in this spread across different analyzed sizes. This is in accordance with ICP-MS/MS data, which showed virtually no differences in $PM_{10}$ and $PM_{2.5}$ samples. SEM/EDX analysis confirmed that this observation was true throughout all

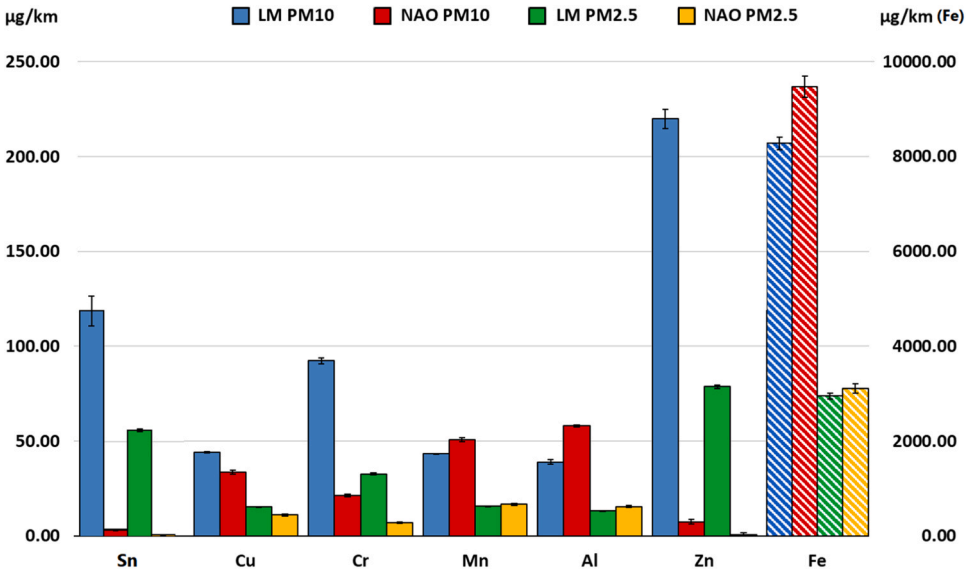


**Fig. 6.** Heavy metal emission factors at the vehicle level. Hatched bars for iron levels are plotted on the right Y-Axis, while solid bars are plotted on the left Y-Axis.

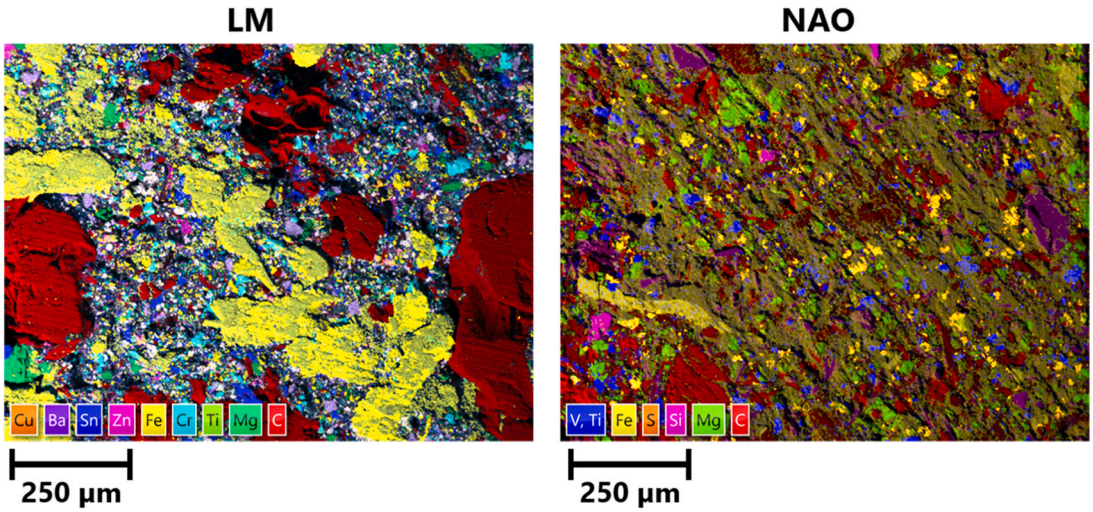


**Fig. 7.** Chemical mapping of bulk brake pad linings at 100 x magnification measured via SEM/EDX.

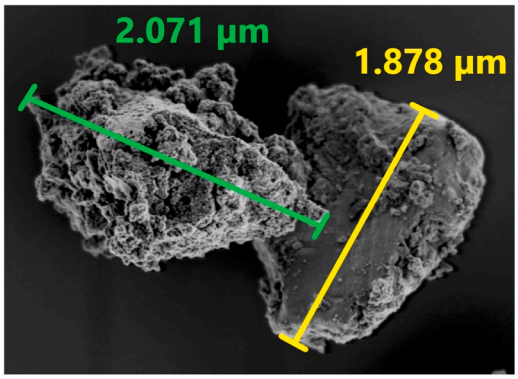


**Fig. 8.** SEM micrograph of spherical (green) and flake-like (yellow) shaped particles commonly found in brake-wear samples. Particles shown originated from the LM brake pad.

size ranges, even down to the ultrafine region, with particles as small as 30 nm consisting of 50 % of iron or more. These small particles are specifically of concern, since particles < 2.5 µm can penetrate deeply into the lung and nanoparticles smaller than 100 nm can eventually reach the bloodstream via entry route through the blood-air-barrier [20, 42], or uptake via the nasal route followed by translocation through the olfactory nerve [21,22].

Interestingly, only a few particles with Fe concentrations of 15 – 30 % and 80 – 90 % were found that matched the initial iron contents of the two analyzed brake pads and the brake disc. Instead, most particles in samples of both pads showed iron concentrations between 50 % and 60 %, which is similar to the average Fe contents found with ICP-MS/MS. This would contradict the hypothesis that the iron contents found with ICP-MS/MS are the result of a mixture of highly iron containing particles from the brake rotor and particles containing lower amounts of Fe from the pads and instead suggest strong changes in the chemical composition for both friction partners. This could potentially also explain the wide range of iron contents, with some effects enhancing the concentration of iron in the pads, like the thermal degradation of the polymeric binding matrix and, on the other hand, effects that lead to emission of particles with lowered Fe content from the brake disc, such as tribo-oxidation. The severance of these effects is visible for the particles F and G in Fig. 9. Particle F featured 74.1 % of Fe and 0.7 % of Mg, while particle G contained 70.6 % of Fe and 1.6 % of Mg. The presence of Mg implies that these particles originated from the NAO pad, since the brake disc contained only 0.01 % of Mg based on ICP-MS results. This would indicate that particles with Fe concentrations of up to 75 % are emitted by a pad that, on average, contained only 17.06 ± 0.66 % of iron (based on ICP-MS/MS). A feasible explanation for this phenomenon would be the chipping of highly Fe containing compounds of the pad, such as the observed steel fibres. As illustrated in Fig. 7 the pads displayed a heterogenous distribution of elements with visible iron rich flakes and fibers that can be abraded by mechanical processes from the tribolayer forming at the friction surface. However, only limited amounts of particles below the average Fe concentrations of the pads were found, which suggest that parts of the pad that are lower in iron still undergo significant changes in their composition, or that they are emitted in larger particles not captured on the filters.

### 3.4. GC-MS/MS analysis

Only 4 substances of the 27 measured PAH in the GC-MS/MS method were found in the filter samples of both brakes at concentrations above the LOD. 1-Methylphenanthrene was detected in LM and NAO samples, at concentrations below the LOQ, while Phenanthrene, Fluoranthene and Pyrene were found at quantifiable concentrations. In total, only 3 and 4 ring structures were observed under the WLTP brake, which is in agreement with results from Alves et al., who reported no detected PAH with five or more benzenic rings [23]. While the WLTP brake provides a wide range of driving conditions for emission measurements, not all real-world scenarios are represented by this cycle. In general- the WLTP brake comprises moderate brake temperatures, which can be exceeded by far in certain situations, such as long deceleration events when driving down a slope. PAH are normally formed at temperatures > 300 °C (Odinga et al., 2021) and can be released during strong braking events, or several braking events in a short succession, where high local temperatures are achieved at the friction interface. Qi and Day demonstrated that brake interface temperatures, which they reported around 400 °C, were substantially higher than average disc temperatures, which ranged around 120 °C (Qi and Day, 2007), by comparing an exposed wire thermocouple to a conventional sliding thermocouple. Especially in mountainous areas where long and steep declines are common, PAH emissions could potentially be significantly higher and also other polycyclic core structures, like 5 ring PAH could be generated.

The NAO pad emitted lower amounts of PAH under tested conditions, even though measured temperatures were higher than for the LM pad and a pad with higher organic content is prone to form more organic degradations products. However, this pad showed an uncommon chemical composition and a higher rotor wear was observed from ICP-MS/MS results. Furthermore, the higher cooling air flow could lead to

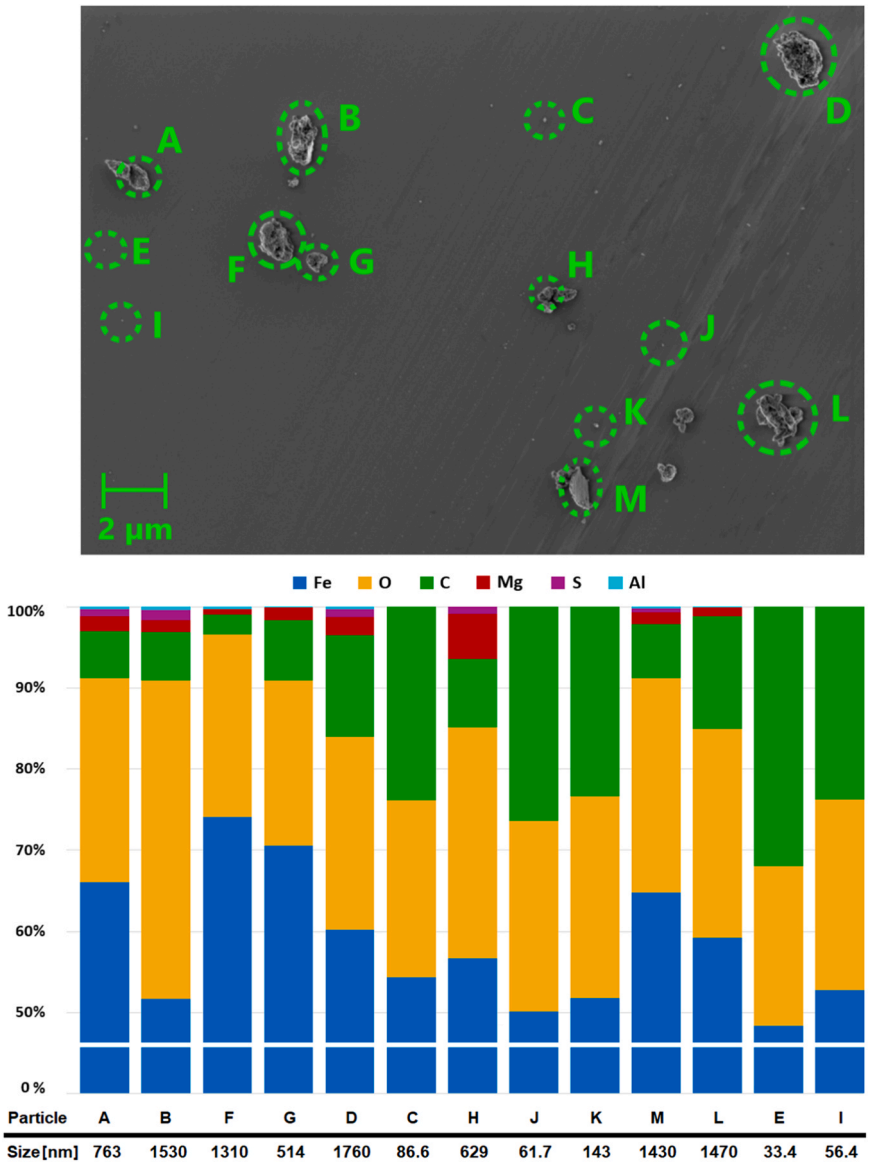


**Fig. 9.** SEM overview and bar chart of elemental compositions, derived from the associated EDX spectra of NAO particles on a Si wafer measured at 5 kV.

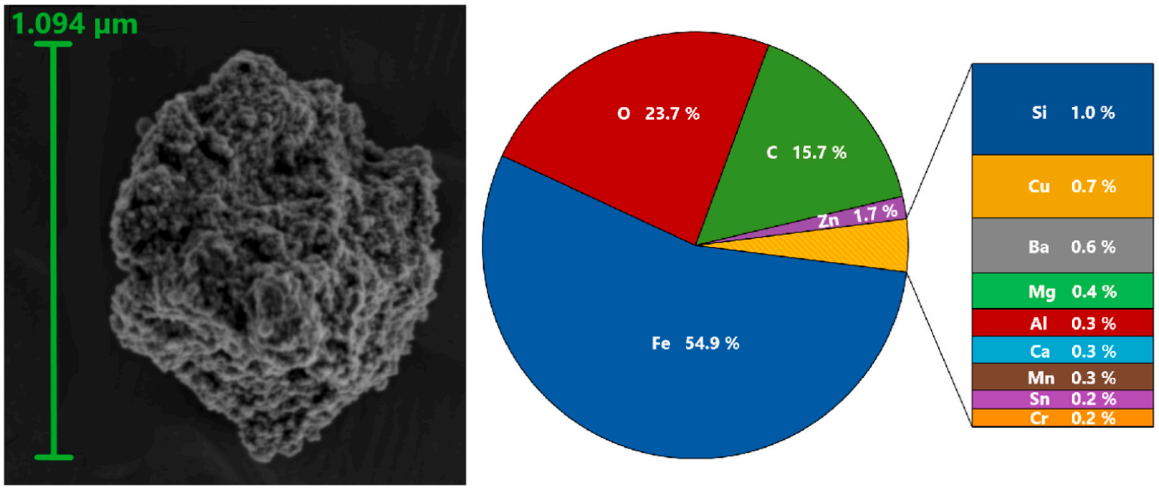


**Fig. 10.** SEM micrograph and pie chart derived from the associated EDX spectrum of a spherical LM particle on a Nb substrate measured at 12 kV.

changes in concentrations for volatile and semi volatile substances due to higher dilution in the tunnel. The $PM_{10}$ and $PM_{2.5}$ emission factors of measured PAH at the vehicle level are listed in Table 4.

## 4. Conclusions

The custom-built brake dynamometer that was utilized in this study and which was tailored to fulfill the requirements of the GTR24 for the measurement of brake emissions as close as possible, yielded reliable and useful results. $PM_{10}$ emission factors at the vehicle level were found at 15.1 ± 0.1 and 16.3 ± 0.4 mg/km, while $PM_{2.5}$ was found at 5.4 ± 0.1 and 7.2 ± 0.2 mg/km for the two tested brake pads. PN emitted from single brakes was measured in the range of $10^9$ #/km with the geometric mean diameter found at 123 (LM pad) and 143 nm (NAO pad) and a second mode for both pads at 86 nm. The emission values of the tested LM pad were in accordance with data from the latest global interlaboratory study, while values obtained for the aftermarket bought NAO pad were unusually high due to an increased iron content of 13.9 %. When comparing the results to the class of LM pads, which fitted better from the chemical compositions the pad yielded comparable result, showing that manufacturers pad type classifications are not always sufficient in estimating emission levels of a certain brake pad.

Chemical analysis of the obtained brake dust revealed highly metallic particles with 54.9–58.1 % of $PM_{10}$ emitted as iron and other heavy metals, such as Cu, Cr, Mn and Zn present in varying concentrations for the two pads. Based on the elemental distribution a high contribution from the wear of the brake disc was observed. Fe emission factors found in this study were 8–9 times higher than previously published studies from non GTR 24 compliant brake dynamometers. In contrast, this study indicates that current Cu emissions from brake pads might be overestimated, based on recent trends in brake pad formulations and differences in emission test setups.

SEM/EDX analysis revealed rough edged surfaces that are typical for abrasion derived particles, with two common morphologies, round and flake-like, displayed throughout all samples. EDX single particle elemental spectra showed high ranges of Fe found between 43 % and 75 % with no noticeable difference within the different size ranges.

Four different PAH species were identified in emissions from both pads, however, no 5-ring or larger PAH structures were found, probably due to the moderate temperatures of the WLTP brake test cycle.

Results from this study highlight the necessity of reducing brake wear emissions and put an emphasis on the importance of physical and chemical characterization of emitted particles. To our knowledge this is the first comprehensive characterization of brake dust, emitted from a GTR24 based brake dynamometer, providing a broader understanding of the chemical composition and the distribution of environmental and health impairing pollutants under standardized test procedures, opening new possibilities for developing policy responses to NEE.

## Environmental Implication

Non-exhaust emissions presently pose the largest portion of particulate emissions from automotive traffic, with brake wear largely contribution to anthropogenic heavy metal emissions, such as Fe and Cu. Many studies have underlined the potential environmental and health impacts of brake wear, however, the detailed physical and chemical properties of brake wear particles under standardized, real-world conditions remain to be studied in-depth. For this reason, particles emitted from a well-controlled custom-built brake dyno were studied under the real-world driving conditions of the WLTP brake cycle to deepen the knowledge on the chemical and physical properties of brake wear.

## CRediT authorship contribution statement

**Mohammad Saraji-Bozorgzad:** Writing – review & editing, Investigation, Conceptualization. **Carsten Neukirchen:** Writing – review & editing, Writing – original draft, Visualization, Validation, Methodology, Investigation, Formal analysis, Data curation, Conceptualization. **Ajit Mudan:** Investigation. **Michael Mäder:** Methodology, Investigation. **Ralf Zimmermann:** Supervision, Project administration, Funding acquisition. **Christian Trapp:** Supervision, Project administration, Funding acquisition. **Thomas Adam:** Supervision, Project administration, Funding acquisition. **Sebastiano Di Bucchianico:** Writing – review & editing, Writing – original draft. **Johannes Becker:** Writing – review & editing, Writing – original draft. **Philipp Czasch:** Methodology.

**Table 4**
PAH emission factors at the vehicle level calculated from $PM_{10}$ and $PM_{2.5}$ filter samples. PAH stated as <LOQ were detected at concentrations above the LOD.

| PAH in ng/km | LM Pad | | NAO Pad | |
|---|---|---|---|---|
| | $PM_{10}$ | $PM_{2.5}$ | $PM_{10}$ | $PM_{2.5}$ |
| Phenanthrene | 44.1 ± 5.6 | < LOQ | 31.9 ± 1.5 | < LOQ |
| 1-Methylphenanthrene | < LOQ | < LOQ | < LOQ | < LOQ |
| Fluoranthene | 32.0 ± 2.8 | 17.5 ± 0.4 | 39.9 ± 0.7 | 18.9 ± 0.6 |
| Pyrene | 14.7 ± 1.3 | 3.8 ± 0.5 | 18.9 ± 0.6 | 10.0 ± 2.2 |

## Declaration of Competing Interest

The authors declare the following financial interests/personal relationships which may be considered as potential competing interests. Thomas Adam reports financial support was provided by dtec.bw - NextGenerationEU. Thomas Adam reports financial support was provided by ULTRHAS - H2020. If there are other authors, they declare that they have no known competing financial interests or personal relationships that could have appeared to influence the work reported in this paper.

## Acknowledgments

Funding: This work was funded by dtec.bw – Digitalization and Technology Research Center of the Bundeswehr [project MORE]. Dtec.bw is funded by the European Union – NextGenerationEU. This research was also supported by the project ULTRHAS – ULtrafine particles from TRansportation – Health Assessment of Sources, a project funded under the EU's Research and Innovation programme Horizon 2020, Grant Agreement No. 955390. We acknowledge financial support by Universität der Bundeswehr München.

GC-MS/MS analysis was supported by student Bastian Lorson, as part of his bachelor thesis.

## Appendix A. Supporting information

Supplementary data associated with this article can be found in the online version at doi:10.1016/j.jhazmat.2024.136609.

## Data availability

Data will be made available on request.

## References

[1] Giechaskiel, B., Maricq, M., Ntziachristos, L., Dardiotis, C., Wang, X., Axmann, H., et al., 2014. Review of motor vehicle particulate emissions sampling and measurement: From smoke and filter mass to particle number. J Aerosol Sci 67, 48–86. ⟨https://www.sciencedirect.com/science/article/pii/S0021850213001961⟩.

[2] Fussell, J.C., Franklin, M., Green, D.C., Gustafsson, M., Harrison, R.M., Hicks, W., et al., 2022. A review of road traffic-derived non-exhaust particles: emissions, physicochemical characteristics, health risks, and mitigation measures. Environ Sci Technol 56 (11), 6813–6835. ⟨https://www.ncbi.nlm.nih.gov/pmc/articles/PMC9178796/⟩.

[3] Piscitello, A., Bianco, C., Casasso, A., Sethi, R., 2021. Non-exhaust traffic emissions: Sources, characterization, and mitigation measures. Sci Total Environ 766, 144440. ⟨https://www.sciencedirect.com/science/article/pii/S0048969720379717⟩.

[4] International Council on clean transportation 2024. Euro 7: The new emission standard for light- and heavy-duty vehicles in the European Union (Accessed 27 August 2024) 2024. ⟨https://theicct.org/wp-content/uploads/2024/03/ID-116-%E2%80%93-Euro-7-standard_final.pdf⟩.

[5] Grigoratos, T., Martini, G., 2014. Non-exhaust traffic related emissions - brake and tyre wear PM: literature review. JRC Sci Policy Rep. https://doi.org/10.2790/21481.

[6] European parliament, 2024. Euro 7: Deal on new EU rules to reduce road transport emissions Parlament.

[7] Grigoratos, T., Martini, G., 2015. Brake wear particle emissions: a review. Environ Sci Pollut Res Int 22 (4), 2491–2504. ⟨https://www.ncbi.nlm.nih.gov/pmc/articles/PMC4315878/⟩.

[8] US EPA, 2015. Copper-Free Brake Initiative | US EPA. ⟨https://www.epa.gov/npdes/copper-free-brake-initiative⟩ (accessed 13 May 2024).

[9] Sinclair Rosselot, K., 2006. Copper released from brake lining wear in the san francisco bay area. Process Profiles. ⟨www.suscon.org/pdfs/bpp/pdfs/BrakeSourcesReportFinal01-30-06a⟩.

[10] Hulskotte, J.H.J., van der Gon, H.A.C.D., Visschedijk, A.J.H., Schaap, M., 2007. Brake wear from vehicles as an important source of diffuse copper pollution. Water Sci Technol 56 (1), 223–231. https://doi.org/10.2166/wst.2007.456.

[11] Barosova, H., Chortarea, S., Peikertova, P., Clift, M.J.D., Petri-Fink, A., Kukutschova, J., et al., 2018. Biological response of an in vitro human 3D lung cell model exposed to brake wear debris varies based on brake pad formulation. Arch Toxicol 92 (7), 2339–2351. https://doi.org/10.1007/s00204-018-2218-8.

[12] Kukutschová, J., Moravec, P., Tomášek, V., Matějka, V., Smolík, J., Schwarz, J., et al., 2011. On airborne nano/micro-sized wear particles released from low-metallic automotive brakes. Environ Pollut (Barking, Essex 1987) 159 (4), 998–1006. ⟨https://www.sciencedirect.com/science/article/pii/S0269749110005476⟩.

[13] Karlsson, H.L., Gustafsson, J., Cronholm, P., Möller, L., 2009. Size-dependent toxicity of metal oxide particles–a comparison between nano- and micrometer size. Toxicol Lett 188 (2), 112–118. ⟨https://www.sciencedirect.com/science/article/pii/S0378427409001611⟩.

[14] Maher, B.A., González-Maciel, A., Reynoso-Robles, R., Torres-Jardón, R., Calderón-Garcidueñas, L., 2020. Iron-rich air pollution nanoparticles: an unrecognised environmental risk factor for myocardial mitochondrial dysfunction and cardiac oxidative stress. Environ Res 188, 109816. https://doi.org/10.1016/j.envres.2020.109816.

[15] Sobolewski, M., Conrad, K., Marvin, E., Eckard, M., Goeke, C.M., Merrill, A.K., et al., 2022. The potential involvement of inhaled iron (Fe) in the neurotoxic effects of ultrafine particulate matter air pollution exposure on brain development in mice. Part Fibre Toxicol 19 (1), 56. https://doi.org/10.1186/s12989-022-00496-5.

[16] Stueckle, T.A., Davidson, D.C., Derk, R., Kornberg, T.G., Schwegler-Berry, D., Pirela, S.V., et al., 2017. Evaluation of tumorigenic potential of CeO2 and Fe2O3 engineered nanoparticles by a human cell in vitro screening model. NanoImpact 6, 39–54. ⟨https://www.sciencedirect.com/science/article/pii/S2452074816300994⟩.

[17] Forest, V., Pourchez, J., 2023. Biological effects of brake wear particles in mammalian models: a systematic review. Sci Total Environ 905, 167266. https://doi.org/10.1016/j.scitotenv.2023.167266.

[18] Gasser, M., Riediker, M., Mueller, L., Perrenoud, A., Blank, F., Gehr, P., et al., 2009. Toxic effects of brake wear particles on epithelial lung cells in vitro. Part Fibre Toxicol 6 (1), 30. ⟨https://particleandfibretoxicology.biomedcentral.com/articles/10.1186/1743-8977-6-30⟩.

[19] Garg, B.D., Cadle, S.H., Mulawa, P.A., Groblicki, P.J., Laroo, C., Parr, G.A., 2000. Brake wear particulate matter emissions. Environ Sci Technol 34 (21), 4463–4469. https://doi.org/10.1021/es001108h.

[20] Bachler, Losert, G., Umehara, S., Goetz, Y., von, N., Rodriguez-Lorenzo, L., Petri-Fink, A., et al., 2015. Translocation of gold nanoparticles across the lung epithelial tissue barrier: Combining in vitro and in silico methods to substitute in vivo experiments. Part Fibre Toxicol 12 (1), 18. ⟨https://particleandfibretoxicology.biomedcentral.com/articles/10.1186/s12989-015-0090-8⟩.

[21] Fortoul, T., V. Rodríguez-Lara, A. González-Villalva, M. Rojas-Lemus, L. Colín-Barenque, P. Bizarro-Nevares et al., 2015. Health Effects of Metals in Particulate Matter. ⟨https://www.semanticscholar.org/paper/Health-Effects-of-Metals-in-Particulate-Matter-Fortoul-Rodr%C3%ADguez-Lara/9e1dcb26db219f654d2ab5e1a1c301fe25a25661#citing-papers⟩.

[22] Hopkins, L.E., Laing, E.A., Peake, J.L., Uyeminami, D., Mack, S.M., Li, X., et al., 2018. Repeated iron-soot exposure and nose-to-brain transport of inhaled ultrafine particles. Toxicol Pathol 46 (1), 75–84. ⟨https://pubmed.ncbi.nlm.nih.gov/28914166/⟩.

[23] Alves, C., Evtyugina, M., Vicente, A., Conca, E., Amato, F., 2021. Organic profiles of brake wear particles. Atmos Res 255, 105557. ⟨https://www.sciencedirect.com/science/article/pii/S0169809521001095⟩.

[24] UNECE, 2024. ECE/TRANS/WP.29/GRPE/2023/4 | UNECE - Proposal for a new UN GTR on Laboratory Measurement of Brake Emissions for Light-Duty Vehicles. ⟨https://unece.org/transport/documents/2023/01/informal-documents/clean-pmp-proposal-amend-ecetranswp29grpe20234⟩ (Accessed 15 March 2024).

[25] VDI 2267 Part 15:2019–12. Determination of suspended matter in ambient air - Measurement of the element concentration after sampling on filters - Determination of Al, As, Ba, Ca, Cd, Co, Cr, Cu, Fe, K, Mg, Mn, Na, Ni, Pb, Sb, Se, Sn, Tl, V, and Zn by GF-AAS, ICP-OES, or ICP-MS.

[26] Neukirchen, C., Meiners, T., Bendl, J., Zimmermann, R., Adam, T., 2024. Automated SEM/EDX imaging for the in-depth characterization of non-exhaust traffic emissions from the Munich subway system. Sci Total Environ 915, 170008. ⟨https://www.sciencedirect.com/science/article/pii/S0048969724001426⟩.

[27] Anastasia A. Andrianova and Bruce D. Quimby, Agilent Technologies. Optimized PAH Analysis Using Triple Quadrupole GC/MS with Hydrogen Carrier (Accessed 24 January 2024). ⟨https://www.agilent.com/cs/library/applications/application-polycyclic-aromatic-hydrocarbons-pah-gcms-gc-tq-gcmsms-5994–2192EN-agilent.pdf⟩.

[28] Grigoratos, T., Mathissen, M., Vedula, R., Mamakos, A., Agudelo, C., Gramstat, S., et al., 2023. Interlaboratory study on brake particle emissions—part i: particulate matter mass emissions. Atmosphere 14 (3), 498. ⟨https://www.mdpi.com/2073-4433/14/3/498⟩.

[29] Mathissen, M., Grigoratos, T., Gramstat, S., Mamakos, A., Vedula, R., Agudelo, C., et al., 2023. Interlaboratory study on brake particle emissions part ii: particle number emissions. Atmosphere 14 (3), 424. ⟨https://www.mdpi.com/2073-4433/14/3/424⟩.

[30] Mathissen, M., Scheer, V., Vogt, R., Benter, T., 2011. Investigation on the potential generation of ultrafine particles from the tire–road interface. Atmos Environ 45 (34), 6172–6179. ⟨https://www.sciencedirect.com/science/article/pii/S1352231011008569⟩.

[31] Perrenoud, A., Gasser, M., Rutishauser, B.R., Gehr, P., Riediker, M., 2010. Characterisation of nanoparticles resulting from different braking behaviours. IJBNN 1 (1), 17. https://doi.org/10.1504/IJBNN.2010.034123.

[32] Wahlström, J., Söderberg, A., Olander, L., Jansson, A., Olofsson, U., 2010. A pin-on-disc simulation of airborne wear particles from disc brakes. Wear 268 (5-6), 763–769. ⟨https://www.sciencedirect.com/science/article/pii/S0043164809006024⟩.

[33] Vasilatou, K., Wälchli, C., Koust, S., Horender, S., Iida, K., Sakurai, H., et al., 2021. Calibration of optical particle size spectrometers against a primary standard: Counting efficiency profile of the TSI Model 3330 OPS and Grimm 11-D monitor in the particle size range from 300 nm to 10 μm. J Aerosol Sci 157, 105818. ⟨https://www.sciencedirect.com/science/article/pii/S0021850221005498⟩.

[34] Olofsson, U., Olander, L., 2013. On the identification of wear modes and transitions using airborne wear particles. Tribology Int 59, 104–113. ⟨https://www.sciencedirect.com/science/article/pii/S0301679×12000382⟩.

[35] Österle, W., Griepentrog, M., Gross, T., Urban, I., 2001. Chemical and microstructural changes induced by friction and wear of brakes. Wear 251 (1-12), 1469–1476. ⟨https://www.sciencedirect.com/science/article/pii/S0043164801007852⟩.

[36] Gad, S.C., 1989. Acute and chronic systemic chromium toxicity. Sci Total Environ 86 (1-2), 149–157. ⟨https://www.sciencedirect.com/science/article/pii/0048969789902015⟩.

[37] Hussain, S., Khan, M., Sheikh, T.M.M., Mumtaz, M.Z., Chohan, T.A., Shamim, S., et al., 2022. Zinc essentiality, toxicity, and its bacterial bioremediation: a comprehensive insight. Front Microbiol 13, 900740. https://doi.org/10.3389/fmicb.2022.900740.

[38] Park, S.B., Cho, K.H., Jung, S., Jang, H., 2009. Tribological properties of brake friction materials with steel fibers. Met Mater Int 15 (1), 27–32. ⟨https://link.springer.com/article/10.1007/s12540-009-0027-6⟩.

[39] Kim, K.I., Lee, H., Kim, J., Oh, K.H., Kim, K.T., 2021. Wear behavior of commercial copper-based aircraft brake pads fabricated under different SPS conditions. Crystals 11 (11), 1298. ⟨https://www.mdpi.com/2073-4352/11/11/1298⟩.

[40] Neis, P.D., Ferreira, N.F., Fekete, G., Matozo, L.T., Masotti, D., 2017. Towards a better understanding of the structures existing on the surface of brake pads. Tribology Int 105, 135–147. ⟨https://www.sciencedirect.com/science/article/pii/S0301679×16303516⟩.

[41] Wahlström, J., Olander, L., Olofsson, U., 2010. Size, shape, and elemental composition of airborne wear particles from disc brake materials. Tribol Lett 38 (1), 15–24. ⟨https://link.springer.com/article/10.1007/s11249-009-9564-x⟩.

[42] Miller, M.R., Raftis, J.B., Langrish, J.P., McLean, S.G., Samutrtai, P., Connell, S.P., et al., 2017. Inhaled nanoparticles accumulate at sites of vascular disease. ACS Nano 11 (5), 4542–4552. https://doi.org/10.1021/acsnano.6b08551.